Materials Advances

ROYAL SOCIETY OF CHEMISTRY

PAPER

View Article Online
View Journal | View Issue

Cite this: *Mater. Adv.*, 2025, 6, 1959

Novel polydopamine/halloysite nanotube-reinforced brushite calcium phosphate cement for bone regeneration with synergistic regulation of mechanical/osteogenic capacity†

Chenhao Wang,[a] Tao Guo,*[a] Yukang Gong,[b] Xintian Wang,[a] Puying An,[a] Jie Zhang,*[a] Zheng Gao,[a] Wenshan Gao,[b] Yuangong Zhang[a] and Feng Liu *[a]

Received 14th November 2024,
Accepted 13th February 2025

DOI: 10.1039/d4ma01124d

rsc.li/materials-advances

Bone regeneration remains a clinical challenge with limited bone substitutes. Brushite calcium phosphate cements (**Bru-CPCs**), possessing good bioactivity and biocompatibility, are one of the widely studied bone graft materials. However, their further application in the long-term remodeling of bone is limited by the low compressive strength. Adding additives has been a promising strategy to solve the above problem. Herein, halloysite nanotubes (**HNTs**) with a unique rod-like structure and excellent biocompatibility were chosen as reinforced materials to fabricate bone repair materials. Inspired by the adhesive proteins in mussels, we modified the **HNTs'** surface with polydopamine (PDA) to improve the inorganic–inorganic phase interfacial interactions between the **HNTs** and **Bru-CPCs**. **Bru-CPCs**, **Bru-CPCs/1.5%HNTs** and **Bru-CPCs/1.5%HNTs@PDA** were fabricated and the mechanical properties and biological activity of the bone repair materials were evaluated in detail. All the results indicated that **Bru-CPCs** incorporated with **1.5 wt% HNTs@PDA** have good compressive strength and osteo-differentiation properties, making them a prospective biomaterial for bone-tissue repair.

Introduction

Large bone defect repair has always been a major challenge in the field of orthopedics.[1–3] Autografts, allografts and xenografts are unable to meet the increasing demand for current clinical needs. Biomaterials have been extensively studied as bone grafts.[4–7] Calcium phosphate cements (CPCs), with low-temperature self-setting, high biocompatibility, and similar constituents to bone, have attracted significant interest as implant materials in bone reconstruction surgery.[8–12] Brushite cements (**Bru-CPCs**) possess superior biodegradability and osteoconductivity, but inferior mechanical strength, rendering them unsuitable for current clinical applications.[13–16] Hence, it's important to improve the mechanical strength of **Bru-CPCs** before using them as bone repair materials.

To date, an efficiency strategy is adding additives, such as polymers (chitosan, cellulose ethers, collagen, starch, *etc.*), metal ions (Fe^{3+}, Zn^{2+}, Mg^{2+}, Si^{2+}, *etc.*) and nanoclay (montmorillonite (MMT), kaolinite (Kaol), LAPONITE® (Lap), halloysite nanotubes (**HNTs**), *etc.*) to CPCs.[17–25] Several studies demonstrated the favorable effects of nanoclay on mechanical strength, cellular adhesion and proliferation. Compared to the other nanoclays, **HNTs** have been widely studied as biomaterials due to their excellent biocompatibility, unique tubular structure, selective drug loading, high mechanical strength and abundant resources.[26–29] Research has explored the function of **HNTs** in modulating osteogenesis.[30–33] Firstly, silicate ions released from **HNTs** stimulate osteogenic differentiation and increase the expression of ALP and OCN genes.[31] Secondly, the nanotube structure of **HNTs** contributes to the stabilization of extracellular proteins, leading to an upregulation of ALP activity.[32] Thirdly, **HNTs** that accumulate within cells promote osteogenesis by directly engaging in protein interactions and intracellular signaling pathways.[33] Zhao *et al.* developed a hierarchical composite scaffold with a deferoxamine delivery system, DFO@GMs-PDA/PCL-**HNTs** (DGPN).[32] They demonstrated that DGPN can promote bone regeneration and accelerate cranial defect healing. Wu *et al.* prepared **HNT**-based bone repair materials.[30] The incorporation of **HNTs** led to an enhanced mechanical performance and upregulated the expression of osteogenic differentiation-related genes. Ji *et al.* developed a porous scaffold for bone regeneration by freeze-drying a mixture of nano-scale drug-loaded halloysite nanotubes (**HNTs**) and gelatin.[34] The scaffold shows a porous

[a] *School of Basic Medical Sciences, Hebei University, Baoding 071002, Hebei, China*
[b] *Affiliated Hospital of Hebei University, Hebei University, Baoding 071002, Hebei, China*

† Electronic supplementary information (ESI) available. See DOI: https://doi.org/10.1039/d4ma01124d

structure and excellent biocompatibility. Compared with the gelatin scaffold, **HNTs** can significantly increase the mechanical properties of the composite scaffold by >300% and match natural cancellous bone. Hence, **HNTs** may be a promising additive for improving the mechanical properties of bone repair materials.

However, the above **HNT**-based bone repair materials were composed of inorganic **HNTs** and organic polymers together. Polymer chains can wrap around the **HNTs**, which benefits the modification of the interfacial interactions between the **HNTs** and the polymer, thereby improving the mechanical properties of bone repair materials.[30,35,36] When introducing **HNTs** into **Bru-CPCs**, the interfacial interaction problem between inorganic **HNTs** and inorganic **Bru-CPCs** may hinder the mechanical properties of **Bru-CPCs**. Polydopamine (PDA) can be papered *via* the self-polymerization of dopamine (DA) in alkaline solution. The strong covalent or noncovalent interactions (hydrogen bonds or stacking interactions, between catechol moieties and substrates) endow extraordinary adhesive properties to PDA. Numerous studies have demonstrated that PDA coating is universal to nearly all substrates, and is like that of mussel adhesive protein, endowing the substrate with biocompatibility, post-functionality and other useful properties.[37] The post-modification of the **HNT** surface with PDA may modify the interfacial interactions between the inorganic **HNTs** and inorganic **Bru-CPCs**.

Herein, aiming to improve the mechanical properties of bone repair materials, a novel **Bru-CPCs/1.5%HNTs** with **HNTs** was developed. The mechanical properties and biological activity of the **Bru-CPCs/1.5%HNTs** scaffold were investigated. Considering the interfacial interactions between **HNTs** and **Bru-CPCs** and the high adhesive property of PDA, the **HNT** surface was then coated by a PDA layer. **Bru-CPCs/1.5%HNTs@PDA** scaffolds were constructed. The effect of **HNTs@PDA** on the mechanical properties and biological activity of the scaffolds were assessed and discussed in detail. All the results demonstrated that adding **HNTs@PDA** can improve the compressive strength and bioactivity properties of **Bru-CPCs/1.5%HNTs@PDA** scaffolds for effective bone cell adhesion and growth, which may be widely used as bone repair materials in the further.

Results and discussion

Characterization of Bru-CPCs@HNTs

Bru-CPCs and modified **Bru-CPCs/HNTs** were first prepared, and the effect of **HNT** content on the mechanical properties of **Bru-CPCs** was investigated, as shown in Fig. 1B and Fig. S1 (ESI†). The results revealed that the mechanical properties increased initially and then decreased with increasing the content of **HNTs**. The optimal mechanical performance was achieved with adding 1.5% **HNTs**, reaching 12.16 MPa. These findings indicate that **HNTs** can enhance the mechanical properties of the modified **Bru-CPCs/HNTs**. But the weak interfacial interaction between **HNTs** and **Bru-CPCs** constrains the potential enhancement of mechanical properties. Additionally,

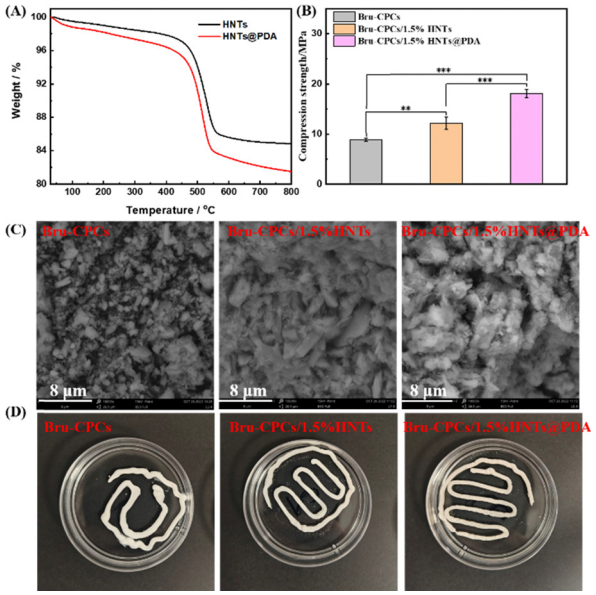

Fig. 1 (A) TGA curves of **HNTs** and **HNTs@PDA**. (B) Compressive strength of CPC scaffolds (incubated at 37 °C and 100% relative humidity for 2 days, $^{**}P < 0.01$, $^{***}P < 0.001$). (C) Morphology of bone repair materials after mineralization. (D) Anti-washout property of the CPC scaffolds. Optical digital images of the CPC scaffolds after being injected into PBS solution and shaken at a speed of 60 rpm at 60 min.

we tested the setting time, pH, and degradation performance, as depicted in Fig. S2 (ESI†). The initial setting time for **Bru-CPCs** was found to be 10 minutes, and the final setting time was 21 minutes. For **Bru-CPCs/1.5%HNTs**, the initial setting time was 9 minutes, and the final setting time was 20 minutes. The addition of **HNTs** had a negligible effect on the setting time. After immersion in SBF solution for 12 hours, the pH of the samples was approximately 5.9. Since SBF was not a buffered system, the pH did not increase to 7.4 within 12 hours. The samples were then incubated for an additional 12 hours, and the pH reached 7.4. The pH values remained almost unchanged around 7.4 for all samples with further incubation. Regarding degradation performance, **Bru-CPCs/1.5%HNTs** exhibited a slightly slower degradation rate compared to **Bru-CPCs**. To further enhance the mechanical properties of **Bru-CPCs** and increase the interfacial interaction between **HNTs** and **Bru-CPCs**, we proposed to modify **HNTs** by introducing polydopamine to prepare **HNTs@PDA**. Subsequently, **HNTs@PDA** will be incorporated into **Bru-CPCs** to further improve their mechanical performance.

Preparation procedures and thermogravimetric analysis and morphology of HNTs@PDA

The preparation process is shown in Scheme 1. Briefly, DA and **HNTs** were stirred in an alkaline environment and a PDA coating was formed on the surface of the **HNTs** by self-polymerization of DA to get **HNTs@PDA**. The morphological characters of **HNTs** and **HNTs@PDA** were revealed by TEM observations, which are shown in Fig. S3 (ESI†). The unmodified **HNTs** exhibit a cylindrical morphology with a distinct, empty central lumen. The **HNT** samples display an open-ended,

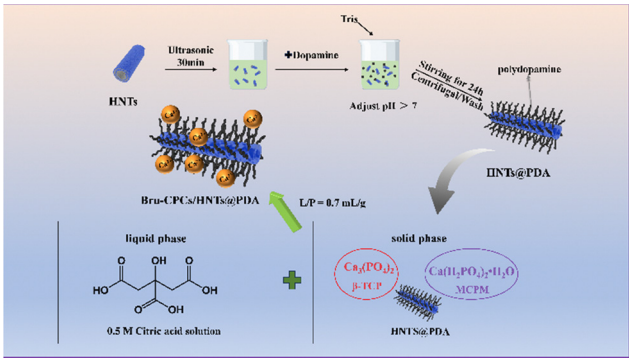

Scheme 1 The preparation process of **HNTs@PDA** and the scaffolds.

hollow cylindrical structure with outer diameters ranging from 32–36 nm and inner diameters spanning 22–25 nm, respectively. The **HNTs** exhibit remarkably clear central channels, a testament to their double-layered nanotube architecture. Upon modification with dopamine, the **HNTs@PDA** display an enlarged outer diameter compared to the unmodified **HNTs**, indicative of a successful PDA coating on the exterior wall of the nanotubes.[38] The **HNTs@PDA** exhibit a notable increase in wall thickness, and their outer surfaces appear roughened and coated with irregular materials, leading to an increase in the diameter of the **HNTs** significantly.[39] The thickness of the **HNTs@PDA** layer (13–19 nm) is larger than that of the PDA layer (8–10 nm), indicating the successful coating of PDA modification.[40]

The corresponding elemental maps displayed in Fig. S4 (ESI†) show the distribution of the constituent calcium element. The calcium mapping of the **Ca-HNTs@PDA** reveals an even distribution of the elemental signal along the entire length of the tube, indicating uniform enrichment of calcium ions. In contrast, the calcium mapping of the **Ca-HNTs** exhibits a random distribution pattern. The surface functionalization achieved through PDA coating enhances the accumulation of calcium ions within the material.[32,41] The strong affinity between calcium ions and the catechol groups present in PDA suggests a significant interfacial interaction, which can contribute to the enhanced interface forces between **HNTs@PDA** and **Bru-CPC**.[42]

We used thermogravimetric analysis to analyze the grafting rate of PDA on **HNTs** (Fig. 1A). As shown in Fig. 1A, the weight decreased upon increasing the temperature from ambient temperature to 800 °C. The weight loss in the temperature range of room temperature to 405 °C was attributed to the adsorbed water and the chemically grafted silane existing in **HNTs**. The weight loss in the temperature range of 405 °C to 535 °C was attributed to the dihydroxylation of structural Al–OH groups of **HNTs**.[43,44] The weight loss of the **HNTs@PDA** increases after coating with PDA. After 800 °C, the remaining weight was 85.0% and 81.6% for **HNTs** and **HNTs@PDA**, respectively, indicating that PDA has been successfully grafted onto **HNTs**. Moreover, a CCK-8 test was performed to investigate the cytocompatibility of the **HNTs** and **HNTs@PDA** by co-culturing MC3T3-E1 cells (Fig. S5, ESI†). The results showed that the number of cells in all groups increased over 24 hours, indicating that the **HNTs** and **HNTs@PDA** had good cell safety. After PDA functionalization, **HNTs** and **HNTs@PDA** were used as a solid additive to be incorporated into **Bru-CPCs** to obtain **Bru-CPCs/1.5%HNTs** and **Bru-CPCs/1.5%HNTs@PDA** (Scheme 1).

Compressive strength, fracture morphology, porosity, and anti-washout property

Compressive strength, fracture morphology, and porosity. The scaffolds were molded to obtain cylindrical forms (Scheme 1). The compressive strength and anti-washout ability of the CPCs, which were critical for actual clinical use, were systematically investigated. The compressive strengths of the pure **Bru-CPCs**, **Bru-CPCs/1.5%HNTs** and **Bru-CPCs/1.5%HNTs@PDA** scaffolds are shown in Fig. 1B and Fig. S1 (ESI†). The compressive strength of **Bru-CPCs** was 8.87 MPa after 2 days of immersion, which was consistent with the literature.[14,45] As the content of **HNTs** increased to 1.5%, the value was increased to 12.16 MPa. The results showed that the addition of **HNTs** can improve the weak compressive strength of bone repair materials. A similar trend was observed for **Bru-CPC/HNTs** and **Bru-CPC/HNTs@PDA** as shown in Fig. S1 (ESI†). When adding **1.5 wt% HNTs@PDA**, the compressive strength of **Bru-CPCs/1.5%HNTs@PDA** further increased to 18.14 MPa, which was about 2-fold higher than that of **Bru-CPCs**. The improvement of the compressive strength of bone repair materials may be attributed to the strong affinity between the catechol moieties of PDA and Ca^{2+} in **Bru-CPCs**. The fracture morphology of the scaffolds was characterized by SEM (Fig. 1C). The fracture morphology of the **Bru-CPCs** was irregular plate-like or flaky brushite crystals with micron to nanometer sizes. **HNTs** can act as crystal nuclei. Hence, with adding **HNTs**, the plate-like crystallization of **Bru-CPCs/1.5%HNTs** was more regular. After introducing **HNTs@PDA**, the crystals of **Bru-CPCs/1.5%HNTs@PDA** are more regularly stacked and the grain size becomes smaller. Some interfaces become blurred. These results may be beneficial to improving the mechanical properties. Fig. S6 (ESI†) exhibits the porosity of the CPCs. The porosity of **Bru-CPCs** was about 42.22 ± 0.75%. The porosities of **Bru-CPCs/1.5%HNTs** and **Bru-CPCs/1.5%HNTs@PDA** were 36.04 ± 0.67% and 38.31 ± 0.71%, respectively. The decrease in the porosity of the CPCs may lead to an increase in compressive strength.

Anti-washout property. The anti-washout property of the CPCs was determined by the appearance integrity after CPCs were injected into the PBS solution as given in Fig. 1D and Fig. S7 (ESI†). CPCs had good continuous shapes when injected into PBS solution. After 60 min of shaking cycles, **Bru-CPCs/1.5%HNTs** slightly disintegrated, while **Bru-CPCs/1.5%HNTs@PDA** showed more complete appearances. This might well be contributed by the chemical chelation of hydroxyl groups with Ca^{2+}.[46,47] The post-modification of the **HNT** surface with PDA modifies the interfacial interactions between inorganic **HNTs** and inorganic **Bru-CPCs** and enhances the anti-washout property of **Bru-CPCs/1.5%HNTs@PDA.**

Adhesive property, CCK-8 analysis, and live/dead staining analysis

Adhesive property. The adhesion and colonization of seed cells on the scaffolds are prerequisites for scaffold-dependent tissue engineering to promote bone regeneration.[48] SEM images showed that the cells started to spread on the surface of **Bru-CPCs**, **Bru-CPCs/1.5%HNTs** and **Bru-CPCs/1.5%HNTs@PDA**. MC3T3-E1 cells on **Bru-CPCs**, **Bru-CPCs/1.5%HNTs** and **Bru-CPCs/1.5%HNTs@PDA** displayed by SEM observation appeared flat with intact, well-defined morphology and extending filopodia (Fig. 2A). This result indicated that all the scaffolds have good cytocompatibility.

CCK-8 analysis. CCK-8 analysis (Fig. 2B) and live/dead staining (Fig. 2C) were used to evaluate the proliferation of MC3T3-E1 cells on the scaffolds. As shown in Fig. 2B, the relative cell proliferation rates were all higher than 70% (the cell survival rate of the control group is defined as 100%), indicating that the cells proliferated well in each group. On the first day of cell culture, the relative cell proliferation rates in the **Bru-CPCs**, **Bru-CPCs/1.5%HNTs**, and **Bru-CPCs/1.5%HNTs@PDA** scaffolds were different, about 101%, 108%, and 112%, respectively. On the 3rd day, the relative cell proliferation rates in the **Bru-CPCs**, **Bru-CPCs/1.5%HNTs**, and **Bru-CPCs/1.5%HNTs@PDA** scaffolds were 124%, 128%, and 131%, respectively. The addition of **HNTs@PDA** increases the cell proliferation rate to a certain extent, which could be attributed to the comprehensive results of improved hydrophilicity, roughness, chemical composition, and morphology of the **HNTs@PDA** coating.[49]

Live/dead staining analysis. The results of the live/dead staining analysis further verified the results of CCK-8 analysis. As shown in Fig. 2C, the living MC3T3-E1 cells were stained green and displayed a normal shape. Compared with the control group and the pure **Bru-CPCs** scaffold, with the addition of **HNTs** and **HNTs@PDA**, the live cell (green fluorescence) density in the **Bru-CPCs/1.5%HNTs** scaffold and the **Bru-CPCs/1.5%HNTs@PDA** scaffold increased and few dead cells (red fluorescence) were observed. All the results demonstrated that the **Bru-CPCs/1.5%HNTs@PDA** scaffold promoted cell adhesion and proliferation and exhibited no adverse effects on cell viability and morphology.

ALP staining, ALP activity, and *In vitro* osteogenesis properties

ALP staining and ALP activity. Alkaline phosphatase (ALP) was an early osteogenic marker, which can reflect the differentiation trend and mineralization ability of osteoblasts.[50] The osteogenic induction of the scaffolds was determined by ALP staining after 7 days of co-cultivation. The ALP expressions of all scaffolds and the control group were positive (Fig. 3A), indicating that all the scaffolds have the potential to promote early osteogenic differentiation. To more intuitively understand the differences in ALP activity of bone repair materials, ALP activity was detected (Fig. 3B). Compared with the control group, the ALP activities of **Bru-CPCs**, **Bru-CPCs/1.5%HNTs**, and **Bru-CPCs/1.5%HNTs@PDA** are all significantly increased.

***In vitro* osteogenesis properties.** To elucidate the moderating effect of **HNTs** and **HNTs@PDA** on osteogenic genes in MC3T3-E1 cells, we performed RT-qPCR for 5 related osteogenesic genes (Col-I, IBSP, OCN, OPN, and Runx2). Fig. 3C shows the expressions of Col-I, IBSP, OCN, OPN, and Runx2 of MC3T3-E1 after co-culturing with **Bru-CPCs**, **Bru-CPCs/1.5%HNTs**, and **Bru-CPCs/1.5%HNTs@PDA**. After culturing for 7 days, the different scaffolds upregulated the expression of 5 related osteogenesic genes to varying degrees. The cells in the group treated with **Bru-CPCs/1.5%HNTs** exhibited a higher

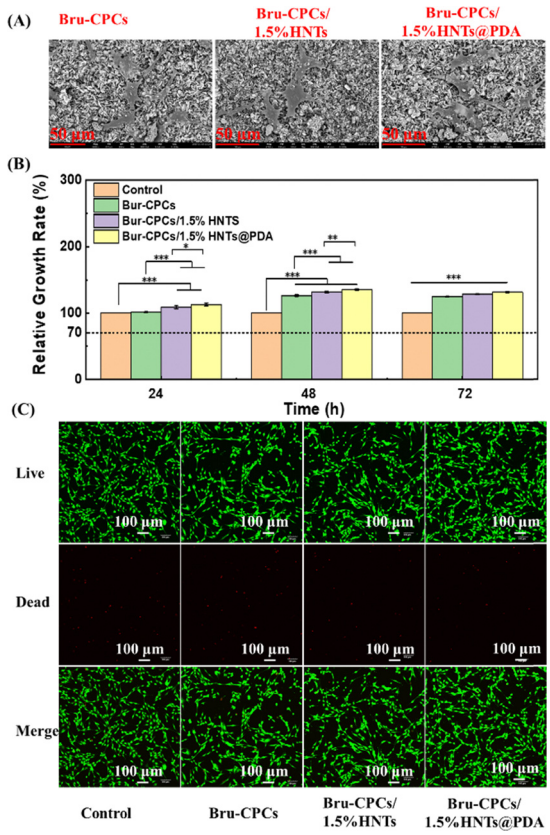

Fig. 2 (A) SEM images of scaffolds co-cultured with cells for 24 h. (B) Cell viability of the scaffolds, in a CCK-8 test (*$P < 0.05$, **$P < 0.01$, ***$P < 0.001$). (C) Live/dead staining images of bone repair materials after co-culturing with cells for 24 hours.

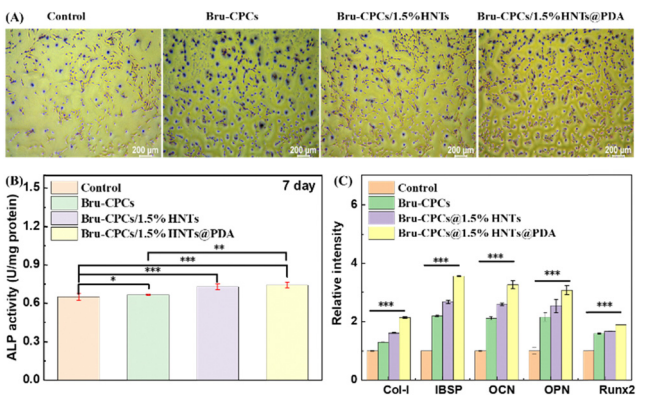

Fig. 3 (A) ALP staining, (B) ALP activity and (C) osteogenesis-related gene expression test of the scaffolds (*$P < 0.05$, **$P < 0.01$, ***$P < 0.001$).

expression of Col-I, IBSP, OCN, OPN and Runx2 than the control group and **Bru-CPCs** group in 7 days. Meanwhile, the expression levels of Col-I, IBSP, OCN and OPN in the **Bru-CPCs/1.5%HNTs@PDA** group had a significant difference with the other groups. Based on the higher expression levels of the four genes, it could be seen that the addition of **HNTs@PDA** into bone repair materials did not impair the osteoconductive function. **Bru-CPCs/1.5%HNTs@PDA** is conducive to the osteogenic differentiation and promotes bone repair.

Conclusions

In this study, **HNTs** were incorporated into **Bru-CPCs** as an additive to enhance the mechanical properties and osteogenic bioactivity of CPCs. The results indicated that the addition of **HNTs** led to an increase in the compressive strength of the CPCs. Additionally, the proliferation and *in vitro* osteogenic differentiation of MC3T3-E1 cells were also improved. The strong affinity between calcium ions and the catechol groups in PDA suggests significant interfacial interaction, which may contribute to the enhanced interface forces between **HNTs@PDA** and **Bru-CPCBru-CPCs**. The interfacial interactions between **HNTs** and **Bru-CPCs** are critical in further augmenting the compressive strength of the CPCs. Subsequently, the **HNT** surface was coated by a PDA layer and **Bru-CPCs/1.5%HNTs@PDA** was fabricated. The **Bru-CPCs/1.5%HNTs@PDA** scaffold exhibited superior compressive strength, cell proliferation, and osteogenic differentiation properties compared to both the **Bru-CPCs** and the **Bru-CPCs/1.5%HNTs** scaffolds. Based on these results, the newly designed **Bru-CPCs/1.5%HNTs@PDA** emerges as a promising candidate for bone-tissue repair applications. This work provides an efficient and universal strategy to design and construct high-performance personalized materials for bone-tissue regeneration. Further research will focus on *in vivo* studies and clinical evaluations, which are essential to ascertain the stability and regenerative potential of the fabricated scaffolds in the context of bone-tissue regeneration.

Data availability

Due to the confidentiality of data, the data including raw files used or analyzed during the current study are available from the corresponding authors on reasonable request.

Conflicts of interest

There are no conflicts to declare.

Acknowledgements

This study was supported by the National Natural Science Foundation of China (No. 22202055), the Natural Science Foundation of Hebei Province, China (No. C2022201038, H2022201017), the Foundation of Hebei Education Department (No. BJK2023004), Foundation of President of Hebei University (No. XZJJ202005), Medical Science Foundation of Hebei University (No. 2021B03), and the ''Advanced Talents Incubation Program of the Hebei University''.

References

1 J. Huang, A. C. Santos, Q. Tan, H. Bai, X. Hu, N. Mamidi and Z. Wu, *J. Nanobiotechnol.*, 2022, **20**, 522.
2 N. Z. Laird, T. M. Acri, K. Tingle and A. K. Salem, *Adv. Drug Delivery Rev.*, 2021, **174**, 613–627.
3 L. Sun, H. Niu, Y. Wu, S. Dong, X. Li, B. Y. S. Kim, C. Liu, Y. Ma, W. Jiang and Y. Yuan, *Bioact. Mater.*, 2024, **35**, 208–227.
4 X. He, Y. Li, D. Zou, H. Zu, W. Li and Y. Zheng, *Bioact. Mater.*, 2024, **39**, 456–478.
5 L. Chen, J. Yang, Z. Cai, Y. Huang, P. Xiao, J. Wang, F. Wang, W. Huang, W. Cui and N. Hu, *Adv. Funct. Mater.*, 2024, **34**, 2314079.
6 J. D. Schwartzman, M. McCall, Y. Ghattas, A. S. Pugazhendhi, F. Wei, C. Ngo, J. Ruiz, S. Seal and M. J. Coathup, *Biomaterials*, 2024, **311**, 122683.
7 M. Li, H. Wu, K. Gao, Y. Wang, J. Hu, Z. Guo, R. Hu, M. Zhang, X. Pang, M. Guo, Y. Liu, L. Zhao, W. He, S. Ding, W. Li and W. Cheng, *Adv. Healthcare Mater.*, 2024, **13**, 2402916.
8 A. Vezenkova and J. Locs, *Bioact. Mater.*, 2022, **17**, 109–124.
9 H. H. K. Xu, P. Wang, L. Wang, C. Bao, Q. Chen, M. D. Weir, L. C. Chow, L. Zhao, X. Zhou and M. A. Reynolds, *Bone Res.*, 2017, **5**, 17056.
10 C. Cui, D. Liu, X. Xie, L. Wang, M. J. Lukic, X. Qiu, W. Chen, J. Shi, Y. Hong, B. Li, Z. Liu and S. Chen, *Composites, Part B*, 2024, **287**, 111812.
11 W. Zhi, X. Wang, D. Sun, T. Chen, B. Yuan, X. Li, X. Chen, J. Wang, Z. Xie, X. Zhu, K. Zhang and X. Zhang, *Bioact. Mater.*, 2022, **11**, 240–253.
12 Y. Feng, D. Wu, J. Knaus, S. Keßler, B. Ni, Z. Chen, J. Avaro, R. Xiong, H. Cölfen and Z. Wang, *Adv. Healthcare Mater.*, 2023, **12**, 2203411.
13 K. Hurle, J. M. Oliveira, R. L. Reis, S. Pina and F. Goetz-Neunhoeffer, *Acta Biomater.*, 2021, **123**, 51–71.
14 W. Gao, H. Wang, R. Liu, X. Ba, K. Deng and F. Liu, *ACS Biomater. Sci. Eng.*, 2024, **10**, 2062–2067.
15 L. Ding, H. Wang, J. Li, D. Liu, J. Bai, Z. Yuan, J. Yang, L. Bian, X. Zhao, B. Li and S. Chen, *Biomater. Sci.*, 2023, **11**, 96–107.
16 G. Tripathi, M. Park, M. Hossain, S. B. Im and B. T. Lee, *Int. J. Biol. Macromol.*, 2022, **221**, 1536–1544.
17 N. Ribeiro, M. Reis, L. Figueiredo, A. Pimenta, L. F. Santos, A. C. Branco, A. P. Alves de Matos, M. Salema-Oom, A. Almeida, M. F. C. Pereira, R. Colaço and A. P. Serro, *Ceram. Int.*, 2022, **48**, 33361–33372.
18 P. A. Krokhicheva, M. A. Goldberg, A. S. Fomin, D. R. Khayrutdinova, O. S. Antonova, A. S. Baikin, A. A. Konovalov, A. V. Leonov, I. V. Mikheev, E. M. Merzlyak, V. A. Kirsanova, I. K. Sviridova, N. S. Sergeeva, S. M. Barinov and V. S. Komlev, *Ceram. Int.*, 2023, **49**, 19249–19264.
19 W. Liu, J. Zhang, P. Weiss, F. Tancret and J.-M. Bouler, *Acta Biomater.*, 2013, **9**, 5740–5750.

20 Y. Wan, H. Ma, Z. Ma, L. Tan and L. Miao, *ACS Biomater. Sci. Eng.*, 2023, **9**, 6084–6093.
21 G. H. Lee, P. Makkar, K. Paul and B. Lee, *Mater. Sci. Eng. C*, 2017, **77**, 713–724.
22 M. Roozbahani and M. Kharaziha, *Biomed. Mater.*, 2019, **14**, 055008.
23 F. Kazemi-Aghdam, V. Jahed, M. Dehghan-Niri, F. Ganji and E. Vasheghani-Farahani, *Carbohydr. Polym.*, 2021, **269**, 118311.
24 L. Tong, Q. Liu, L. Xiong, P. Wang, M. Zhao, X. Li, J. Liang, Y. Fan, X. Zhang and Y. Sun, *Sci. China Mater.*, 2024, **67**, 2067–2079.
25 F. Doustdar, A. Olad and M. Ghorbani, *Carbohydr. Polym.*, 2022, **282**, 119127.
26 J. Liao, H. Wang, N. Liu and H. Yang, *Adv. Colloid Interface Sci.*, 2023, **311**, 102812.
27 E. Torres, V. Fombuena, A. Vallés-Lluch and T. Ellingham, *Mater. Sci. Eng., C*, 2017, **75**, 418–424.
28 J. Varshosaz, Z. S. Sajadi-Javan, M. Kouhi and M. Mirian, *Int. J. Biol. Macromol.*, 2021, **192**, 869–882.
29 J. Zheng, F. Wu, H. Li and M. Liu, *Mater. Sci. Eng., C*, 2019, **105**, 110072.
30 K. Huang, Q. Ou, Y. Xie, X. Chen, Y. Fang, C. Huang, Y. Wang, Z. Gu and J. Wu, *ACS Biomater. Sci. Eng.*, 2019, **5**, 4037–4047.
31 D. M. Reffitt, N. Ogston, R. Jugdaohsingh, H. F. J. Cheung, B. A. J. Evans, R. P. H. Thompson, J. J. Powell and G. N. Hampson, *Bone*, 2003, **32**, 127–135.
32 R. Wang, X. Zha, J. Chen, R. Fu, Y. Fu, J. Xiang, W. Yang and L. Zhao, *Adv. Healthcare Mater.*, 2024, **13**, 2304232.
33 M. Mousa, N. D. Evans, R. O. C. Oreffo and J. I. Dawson, *Biomaterials*, 2018, **159**, 204–214.
34 L. Ji, W. Qiao, Y. Zhang, H. Wu, S. Miao, Z. Cheng, Q. Gong, J. Liang and A. Zhu, *Mater. Sci. Eng., C*, 2017, **78**, 362–369.
35 Y. Zhou, X. Gao, M. Zhao, L. Li and M. Liu, *Compos. Sci. Technol.*, 2024, **250**, 110537.
36 Q. Ou, K. Huang, C. Fu, C. Huang, Y. Fang, Z. Gu, J. Wu and Y. Wang, *Chem. Eng. J.*, 2020, **382**, 123019.
37 J. Wang, Y. Cui, B. Zhang, S. Sun, H. Xu, M. Yao, D. Wu and Y. Wang, *Mater. Des.*, 2024, **238**, 112655.
38 S. Choi, S. Chaudhari, H. Shin, K. Cho, D. Lee, M. Shon, S. Nam and Y. Park, *J. Ind. Eng. Chem.*, 2022, **105**, 158–170.
39 D. Gnanasekaran, A. Shanavas, W. W. Focke and R. Sadiku, *RSC Adv.*, 2015, **5**, 11272–11283.
40 C. Chao, J. Liu, J. Wang, Y. Zhang, B. Zhang, Y. Zhang, X. Xiang and R. Chen, *ACS Appl. Mater. Interfaces*, 2013, **5**, 10559–10564.
41 S. Kim and C. B. Park, *Biomaterials*, 2010, **31**, 6628–6634.
42 N. Holten-Andersen, T. E. Mates, M. S. Toprak, G. D. Stucky, F. W. Zok and J. H. Waite, *Langmuir*, 2009, **25**, 3323–3326.
43 Z. Wang, H. Wang, J. Liu and Y. Zhang, *Desalination*, 2014, **344**, 313–320.
44 Y. Zhang, R. Meng, J. Zhou, X. Liu and W. Guo, *Colloids Surf., A*, 2022, **648**, 129378.
45 H.-J. Lee, B. Kim, A. R. Padalhin and B.-T. Lee, *Mater. Sci. Eng., C*, 2019, **94**, 385–392.
46 H. Shi, X. Ye, J. Zhang and J. Ye, *ACS Biomater. Sci. Eng.*, 2019, **5**, 262–271.
47 L. Ding, H. Wang, W. Zhang, J. Li, D. Liu, F. Han, S. Chen and B. Li, *J. Mater. Chem. B*, 2021, **9**, 6802–6810.
48 B. G. Sengers, M. Taylor, C. P. Please and R. O. C. Oreffo, *Biomaterials*, 2007, **28**, 1926–1940.
49 Y. Yu, X. Li, J. Li, D. Li, Q. Wang and W. Teng, *Mater. Sci. Eng., C*, 2021, **131**, 112473.
50 Y. Wang, C. J. E. Davey, K. van der Maas, R.-J. van Putten, A. Tietema, J. R. Parsons and G.-J. M. Gruter, *Sci. Total Environ.*, 2022, **815**, 152781.